Journal of Energy Storage 162 (2026) 122105

Contents lists available at ScienceDirect

Journal of Energy Storage

journal homepage: www.elsevier.com/locate/est

Research papers

# Heat flux and energy analysis of thermal bridge behaviour at wall and floor panel junctions in prefabricated cold storage systems: Experimental and numerical study

Gulenay Alevay Kilic [a,*], Enver Yalcin [b]

[a] Department of Electrical and Energy, Yalova Vocational School, Yalova University, Yalova, 77200, Turkiye
[b] Department of Mechanical Engineering, Engineering Faculty, Balikesir University, Balikesir, 10145, Turkiye

ARTICLE INFO

*Keywords:*
Thermal bridges
Heat flux
Cold storage
Junction geometry
Energy performance
Prefabricated panels

ABSTRACT

Thermal bridges at panel junctions constitute a critical weakness in prefabricated cold storage systems, where localized heat transfer adversely affects energy efficiency, condensation control, and operational reliability. Although modular polyurethane sandwich panels are widely adopted, the thermal behaviour of junction geometries in cold storage environments remains insufficiently addressed in current standards. This study investigates thermal bridge formation and mitigation in prefabricated cold room panels, with particular emphasis on wall–wall, wall–ceiling, and wall–floor junctions. A combined experimental–numerical methodology is employed. Infrared thermography measurements performed on a cold storage test unit at an internal temperature of 273 K are used to validate high-resolution finite element models, achieving a numerical–experimental agreement of approximately 98%. The validated model is subsequently applied to six different joint configurations with identical material properties and boundary conditions, analysed under internal temperatures of 273 K and 255 K. Thermal performance is evaluated using temperature distributions, heat flux vector fields, and dimensionless parameters including normalised temperature and relative heat flux ratio ($q^*$). While average surface temperatures across different joint geometries are found to vary within a narrow range around 285 K at 273 K internal conditions, the corresponding heat flux values exhibit pronounced differences. Reference flat and Z-type joints show the highest heat flux levels, reaching $\sim$10 W/m$^2$ at 273 K and $\sim$13 W/m$^2$ at 255 K, indicating strong thermal short-circuit behaviour. In contrast, stepped and interlocking joint configurations reduce the effective heat flux to below 8 W/m$^2$ at 273 K and approximately 12 W/m$^2$ at 255 K, accompanied by more homogeneous thermal fields. The results demonstrate that surface temperature alone is insufficient to characterize thermal bridge severity, whereas heat flux intensity and relative heat flux provide more sensitive and geometry-dependent performance indicators. The results indicate that thermal bridge mitigation in cold storage envelopes can be effectively enhanced through geometric optimization of panel joints, while maintaining identical panel thickness and material properties. Furthermore, the proposed heat-flux-based, dimensionless evaluation framework provides a physically grounded tool for comparative assessment of joint designs and may support future improvements in cold storage design practices.

## 1. Introduction

Cold storage systems constitute a vital component of modern refrigeration infrastructure, particularly in ensuring the preservation and safety of perishable goods throughout the cold chain. With increasing global demand for reliable storage and transport of temperature-sensitive products, coupled with the steady rise in energy costs, optimizing the thermal performance of cold rooms has become a critical engineering objective. The regulatory framework established by the Agreement on the International Carriage of Perishable Foodstuffs and Special Equipment to Be Used for Carriage (ATP), adopted into Turkish legislation in 2012, has further driven the development of refrigerated storage and transport systems. This agreement mandates continuous thermal control during the shipment of various food categories such as meat, dairy, seafood, frozen meals, and fresh produce, highlighting the essential role of thermal reliability in cold chain

* Corresponding author.
*E-mail addresses:* gulenay.kilic@yalova.edu.tr (G.A. Kilic), eyalcin@balikesir.edu.tr (E. Yalcin).

https://doi.org/10.1016/j.est.2026.122105
Received 19 January 2026; Received in revised form 22 February 2026; Accepted 2 April 2026
Available online 8 April 2026

systems [1].

Among the commonly adopted construction methods, prefabricated polyurethane insulation panels are widely used due to their modularity, ease of assembly, and favorable thermal properties. Nevertheless, the occurrence of geometric discontinuities or incorrect assembly details at junctions can lead to thermal bridging. These localized regions of elevated thermal conductivity compromise the uniformity of the insulation layer, resulting in increased energy consumption, prolonged refrigeration cycles, and surface condensation. Over time, these issues may lead to corrosion, microbial growth, and degradation of structural and hygienic performance in cold storage environments. Thermal bridges typically occur where different construction materials intersect or where continuity in thermal insulation is interrupted. These irregularities give rise to localized two-dimensional or three-dimensional heat transfer paths [2].

Experimental and numerical studies have shown that geometric discontinuities, such as 10 mm and 20 mm thick mortar joints between wall components, can increase localized heat flux by approximately 62% and 103%, respectively, depending on joint thickness and surface coverage [3]. Alternative materials including cork-based and mushroom-based mortars have demonstrated improved performance in mitigating these effects [4]. In reinforced concrete structures, regions such as beam-slab intersections and balcony extensions often exhibit significantly higher heat transfer rates, with differences reaching 58% across seasonal thermal loads [5,6]. Even more pronounced are steel junctions, such as door-wall intersections, where heat loss has been reported to be up to 28 times greater than adjacent insulated areas [7].

Accurate identification and evaluation of thermal bridges require advanced numerical approaches. Methods such as finite element, finite difference, and finite volume modelling offer detailed representations of temperature distributions and heat flow in complex geometries [8]. However, the accuracy of these simulations is highly sensitive to the specification of boundary conditions, geometric detail, and material properties. Prior studies have highlighted inconsistencies between simulation results and experimental data when simplified standard-based assumptions are applied, as observed with ISO 10211 geometries [9,10]. Despite these challenges, when properly implemented, numerical methods provide a robust framework for evaluating thermal bridge behaviour [11–13].

A considerable body of research has been devoted to understanding the formation mechanisms, heat transfer implications, and mitigation strategies related to thermal bridges in residential and commercial buildings [14–21]. These studies have provided valuable insights into the role of junction geometries, material interfaces, and insulation continuity in overall energy performance. While these studies highlight the combined influence of material properties, insulation continuity, and construction details, the present study specifically isolates the effect of joint geometry by maintaining identical material properties and boundary conditions across all configurations. However, despite their relevance, such investigations rarely extend to cold storage environments, particularly those operating at medium or low temperatures. The unique thermal and structural demands of cold rooms and refrigerated transport systems present distinct challenges that remain underrepresented in current literature. In such systems, even minor thermal discontinuities can lead to substantial energy losses, surface condensation, or temperature instability, directly affecting product safety and operational reliability. Therefore, addressing thermal bridges in cold stores is not only an energy efficiency issue but also a critical factor for hygienic and functional performance. Despite the growing awareness of thermal bridge effects, current regulatory frameworks remain insufficient to fully address the challenges specific to cold storage structures. Most existing standards, including TS EN 13496 through TS EN 13500 and TS EN ISO 13370:2009, are primarily developed for conventional buildings and focus on general insulation practices rather than the junction-specific complexities of refrigerated environments. In Turkiye, TS 4855 governs the design of cold storage systems but does not explicitly include guidelines or requirements for thermal bridge analysis. Moreover, even TS EN ISO 10211, which introduces the thermal coupling coefficient L2D, has shown limitations in accurately capturing heat flow behaviour at complex junctions such as parapet walls and roof-to-wall connections [22,23]. These challenges emphasize the need for targeted research focusing on junction-level heat transfer in cold storage applications, where conventional insulation strategies and modelling assumptions often fall short.

Prefabricated modular cold storage units constructed with metal-faced polyurethane panels certified under European Technical Approval ETA 10/0376 [24] and standard EN 14509 [25] offer high thermal insulation efficiency and flexible installation advantages under standard test conditions. However, application experience shows that thermal bridges can still occur, particularly at structural joints where metal locking elements disrupt the insulation continuity. The forthcoming prEN 14509-1 and prEN 14509-2 standards [26–30] place greater emphasis on improving structural performance and thermal continuity at panel joints. In this context, the development and implementation of advanced joint designs that go beyond current standard panel configurations are becoming important for increasing the energy efficiency and operational reliability of cold storage facilities.

In light of these gaps, the present study investigates the formation and mitigation of thermal bridges in a cold storage facility constructed with prefabricated polyurethane panels. A combination of experimental observations and high-resolution two-dimensional and three-dimensional finite element simulations is used to analyze heat transfer at wall-wall, wall-ceiling, and wall-floor junctions. The effectiveness of proposed assembly modifications is evaluated based on improvements in surface temperature distributions and the reduction of condensation risk. The outcomes of this study are intended to support the development of more thermally efficient and structurally reliable cold storage solutions.

## 2. Experimental and numerical methodology

This study aims to comparatively evaluate the thermal performance of different panel joint geometries used in prefabricated modular cold room panels. Initially, in the experimental phase, a panel thickness of 60 mm was considered, and numerical modelling studies were conducted using thermal camera measurements taken at an internal ambient temperature of 0 °C and − 18 °C as a reference. The numerical temperature distribution results obtained using ANSYS Workbench 2025 R1 software [31] were compared with the experimental measurements, and it was determined that the numerical model provided 98.2% accuracy. This validated model was scaled to a panel thickness of 120 mm and used in comprehensive thermal and heat flux analyses for six different structure configurations at indoor temperatures of 0 °C and −18 °C.

Fig. 1 presents the measurement and modelling outputs for the cold storage room and panel joint area, which formed the basis of the experimental validation process. Fig. 1a shows the general view of the test room constructed with 60 mm thick polyurethane-filled sandwich panels. The chamber was tested under conditions where the internal ambient temperature was maintained at 0 °C. Fig. 1b shows the thermal imaging corresponding to the relevant measurement condition. The image highlights significant temperature deviations occurring at the door-wall junction, which has been identified as a potential thermal bridge. Surface temperature measurements were performed using a Testo 872 thermal imaging camera. According to the manufacturer's specifications, the device provides an infrared resolution of 320 × 240 pixels (up to 640 × 480 pixels with SuperResolution), a thermal sensitivity of approximately 0.05 K, and a typical temperature measurement accuracy of ±2 °C. Point temperature measurements were recorded using a Testo 176 T4 data logger equipped with thermocouple inputs; the measurement accuracy and resolution of the system were specified based on the manufacturer's official technical documentation.

The 3D geometric structure forming the basis of the numerical

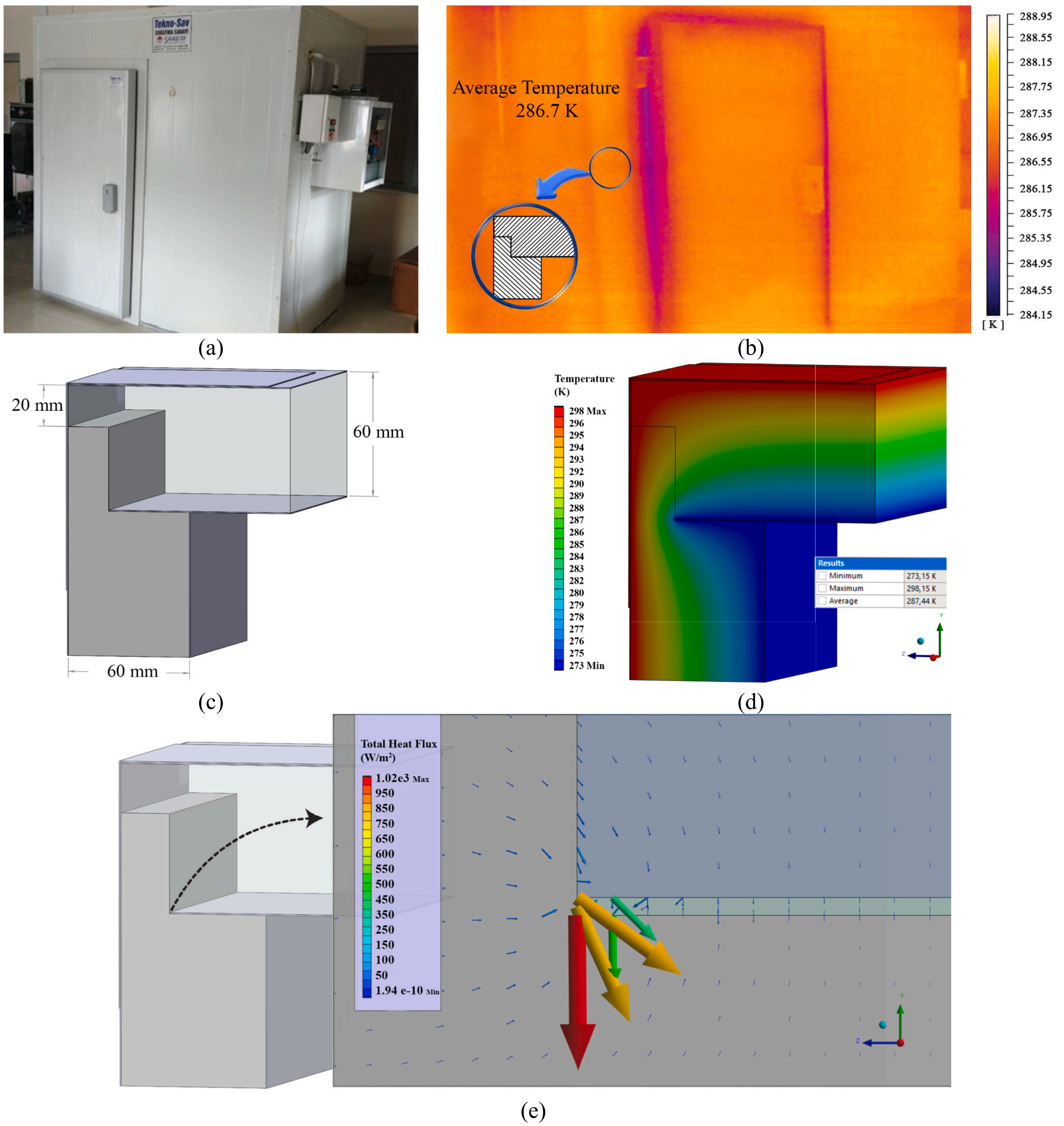


**Fig. 1.** Experimental and numerical validation of thermal bridging at cold room panel junctions: (a) Modular cold storage unit used in the experimental setup; (b) Infrared thermography showing localized thermal anomalies at the door-wall interface under 0 °C set-point; (c) 3D representation of the 60 mm thick joint configuration used for modelling; (d) Numerical temperature distribution obtained via steady-state thermal simulation; (e) Heat flux vector field illustrating localized conduction pathways at the discontinuity.

modelling is presented in Fig. 1c. This structure represents the characteristic Z-type interlocking connection at the panel joint area. Fig. 1d shows the temperature distribution obtained under a constant indoor temperature of 0 °C, with heat transfer intensity clearly observable at the edges in contact with the outdoor environment. Fig. 1e shows the heat flux vector field obtained from the validated model of the same structure. The direction and intensity of the vectors reveal that the heat flux is locally concentrated in the joint area and that this area acts as an effective thermal bridge.

During the model validation process, the experimentally obtained temperature profile was compared with the numerical analysis results. Fig. 2 shows the position-dependent variation of temperature data taken horizontally from the 60 mm thick panel joint area. The experimental (red dots) and numerical (green circles) data are seen to coincide to a high degree along the measurement line. The low average deviation indicates that the numerical model represents the physical behaviour

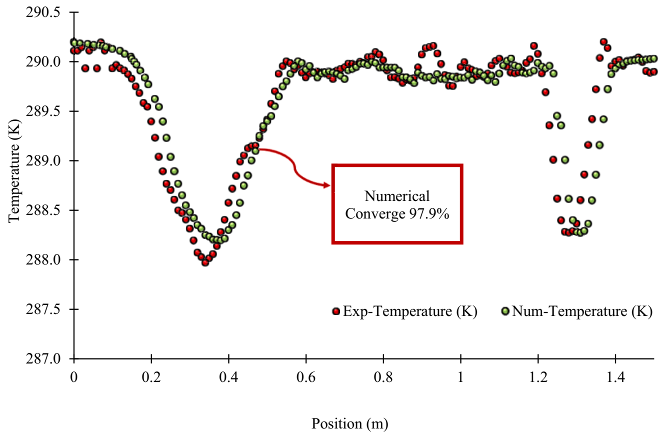


**Fig. 2.** Experimental and numerical temperature distributions along the panel junction as a function of position.

with good accuracy. Based on the comparison between experimental and numerical temperature values, the average relative error was approximately 2.1%, corresponding to an agreement level of 97.9%, which supports the suitability of the numerical model for further analyses.

In order to perform a comparative analysis in the study, six different panel joint models, each with an insulation thickness of 120 mm, were created. These models, summarised in Table 1, considered different levels of structural complexity, such as *Z*-joints, interlocking and multi-step connections. In all multi-step connections, the step depth was determined to be approximately 23% of the panel thickness, in line with typical production *The numerical framework is restricted to steady-state conductive heat transfer and does not explicitly incorporate moisture transport or humidity-dependent phenomena. Accordingly, condensation-related interpretations are limited to indirect assessments based on surface temperature distributions and heat-flux-based indicators under prescribed internal temperature conditions.* In the present study, a step depth corresponding to approximately 23% of the panel thickness was adopted, based on typical design practices in modular cold storage panel manufacturing [28–30]. This ratio allows for a comparative evaluation of the geometric parameters affecting thermal bridge formation.

Six different joint configurations have been created based on 120 mm thick panels. The flat butt joint model presented in Fig. 3(a) is defined as the reference structure, which does not involve any locking or overlap. The configuration in Fig. 3b represents the *Z*-joint type classic lap joint structure. Fig. 3c and d show the single lap overlap joint and double-lap overlap joint structures, respectively, and include details of panels overlapping in steps in the horizontal plane. Fig. 3e and f, which have more complex geometries, present the double-step interlocking joint and multi-step interlocking joint structures, respectively. In these two models, multiple stepped transitions are defined on the panel joint surfaces in both the horizontal and vertical planes, aiming to extend the conductive path and break the thermal flow. All models were comparatively analysed in terms of thermal bridge effect and heat flux distribution at both 0 °C and − 18 °C indoor temperatures.

**Table 1**
Geometric specifications of panel joint configurations used in numerical analysis.

| Model | Type of model | Panel thickness (mm) | Step depth (mm) | Ratio (r = d/$t_{panel}$) |
|---|---|---|---|---|
| Model 1 | Flat butt joint | 120 | – | – |
| Model 2 | *Z*-joint | 120 | 30 | ~0.25 |
| Model 3 | Single lap overlap joint | 120 | 30 | ~0.25 |
| Model 4 | Double-lap overlap joint | 120 | 30 | ~0.25 |
| Model 5 | Double-step interlocking joint | 120 | 30 | ~0.25 |
| Model 6 | Multi-step interlocking joint | 120 | 30 | ~0.23 |

### *2.1. Mesh independence study*

A network structure sensitivity analysis was performed to assess the influence of mesh density on the numerical results. Fig. 4 shows how the temperature values obtained at a characteristic monitoring point near the panel junction region vary under different network densities. As the number of elements was increased from approximately 0.5 million to values exceeding 5 million, the calculated temperature value converged asymptotically, and the difference between the last two network levels fell below 0.2%. This difference was considered sufficient to demonstrate that network independence had been achieved. The selected third network structure was determined by considering both computation time and accuracy. All numerical simulations were conducted under steady-state thermal conditions, and the solution procedure was therefore independent of temporal discretization.

Fig. 5 presents a cross-sectional view of the joint region of the mesh structure. Local mesh refinement has been applied in regions where thermal gradients are concentrated, thereby enabling more accurate modelling of thermal bridging effects. This has allowed for the detailed capture of two-dimensional and three-dimensional heat transfer pathways formed in panel joint regions, enabling the accurate representation of abrupt changes in temperature distribution. Furthermore, the fine mesh structure has increased numerical consistency in critical parameters such as surface temperatures and local heat flux vectors. The mesh resolution used in the modelling process has kept the computational load at a reasonable level while maximising the ability to represent physical reality.

### *2.2. Wall–floor junction modelling and analysis*

In prefabricated modular cold room systems, the wall-floor junction is considered one of the most critical areas for thermal bridging formation, as it represents the interface between the vertical structural elements and the floor. Therefore, in addition to wall-wall and wall-ceiling junctions, wall-floor junctions were also addressed as a separate analysis topic in the study.

The reference geometric structure for the wall–floor joint, shown in Fig. 6, was created according to the typical rotary hook locking detail defined in the ETA-10/0376 standard [24]. In addition to this reference model, two-stage and multi-stage interlocking joint geometries, which showed the best thermal performance in the analyses performed for wall-ceiling joints, were adapted to the floor joint to create alternative models.

All wall–floor joint models were analysed under steady-state conditions using the same material properties, boundary conditions, and mesh density, consistent with the validated numerical modelling approach used for wall–wall and wall–ceiling joints. The analyses were performed for two different scenarios where the internal ambient temperature was set to 255 K and 273 K; thermal behaviour was evaluated through temperature distributions, heat flux vector fields, and average heat flux density. This approach enabled a direct comparison of the thermal performance of the reference and developed wall-floor joints. To understand the thermal bridge behaviour in wall–floor junctions, the local concentration of heat flow in the reference junction geometry was first examined. Accordingly, the local heat flux distribution for the model representing the reference model was analysed in detail under conditions where the indoor temperature was 273 K.

To provide an initial illustration of the thermal bridge behaviour at wall–floor junctions, the spatial distribution of heat flux in the reference joint geometry was examined. Accordingly, the heat flux field for Model

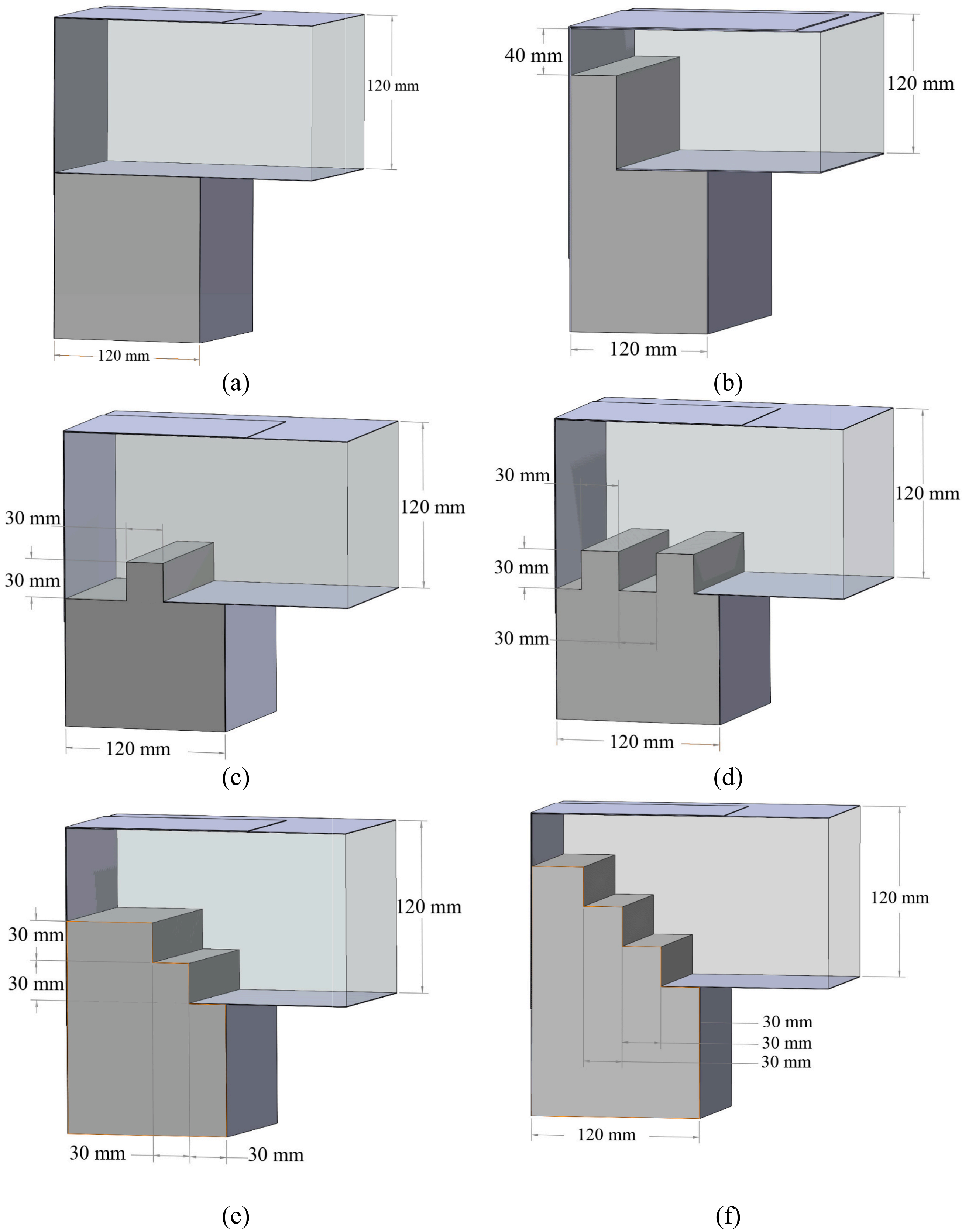


**Fig. 3.** Geometric configurations of modular cold room panel joints with 120 mm insulation thickness: (a) flat butt joint, (b) single-lap overlap, (c) double-lap overlap, (d) triple-step overlap, (e) double step interlocking joint, (f) Multi-step interlocking joint.

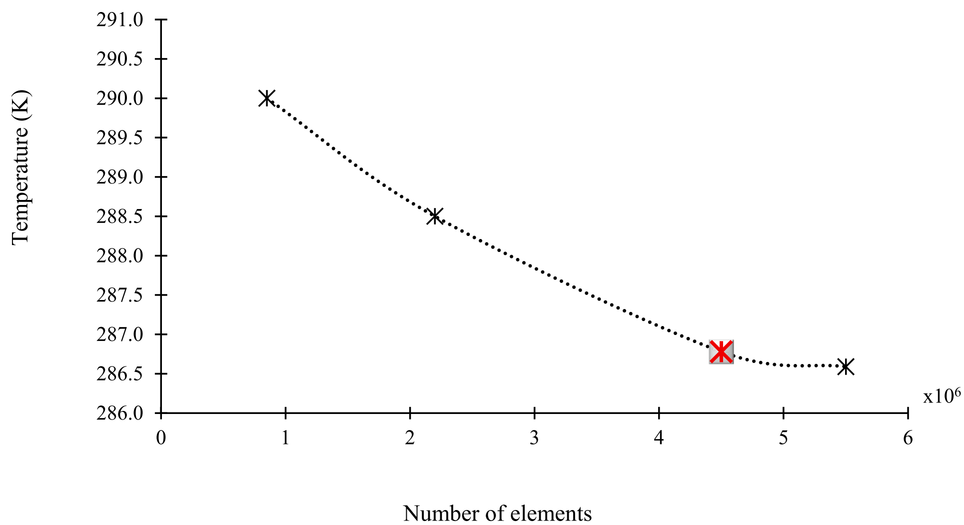


**Fig. 4.** Influence of mesh density on temperature distribution.

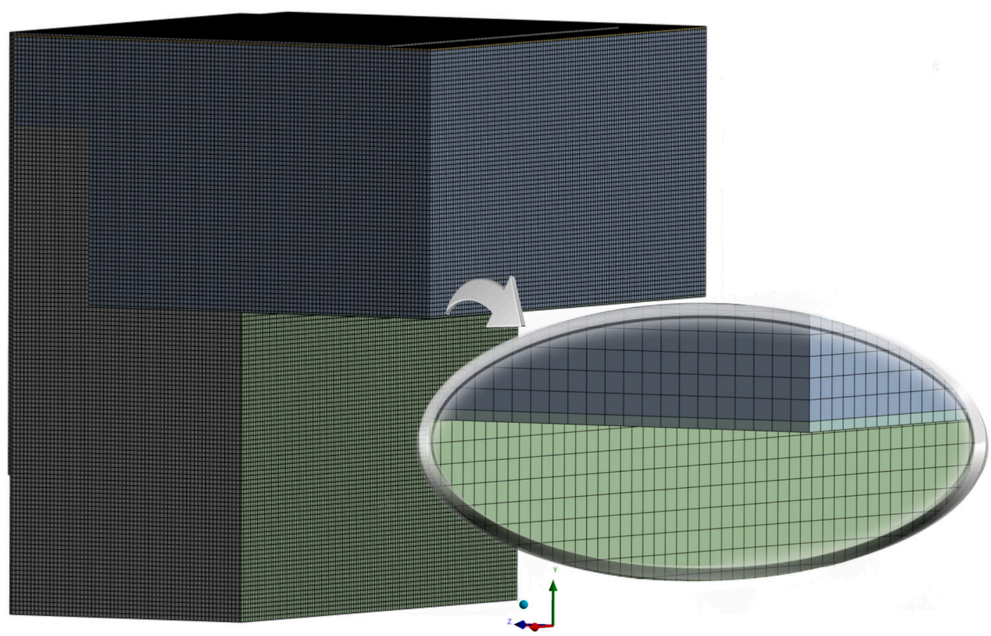

**Fig. 5.** Detailed cross-sectional view of the refined computational mesh.

1, representing the reference configuration under an internal ambient temperature of 273 K, was analysed. As shown in Fig. 7, the geometric discontinuity at the junction region does not lead to a purely localized heat transfer path confined to the immediate vicinity of the joint. Instead, the heat flux is redistributed over a wider area and propagates along the adjacent wall and floor components, indicating that the thermal load induced by the junction geometry is transferred to the surrounding structural elements. This spatial spreading of heat flux suggests that the influence of the thermal bridge extends beyond a single point, resulting in a distributed thermal effect within the wall–floor assembly. This distribution pattern highlights that junction-induced thermal effects are more appropriately interpreted at the assembly level rather than as a purely pointwise phenomenon.

Fig. 8 presents the front views of three different geometric configurations analysed for the wall–floor joint in prefabricated cold room panels. Model 1 (Fig. 8a–b) represents the reference geometry based on the ETA-10/0376 standard. Model 4 (Fig. 8c–d) incorporates the adapted floor application of the validated double-step overlapping joint method for wall–ceiling joints; it extends the transmission path with a step depth of 30 mm (25% r). Model 6 (Fig. 8e–f) increases thermal resistance and maximises insulation continuity by creating fractured transmission paths thanks to its multi-step overlapping structure. Such local heat flux concentrations are qualitatively consistent with the thermal bridge mechanisms observed in the classical panel–floor joint details reported in the literature [3,6,7,10,24].

### 2.3. Governing equations

The thermal behaviour of cold storage wall assemblies was modeled under steady-state conditions, assuming no internal heat generation, convection, or radiation within the solid domain. The formulation is based on the conservation of energy and Fourier's law of heat conduction, which governs the diffusive transport of thermal energy in solids. The general 3D form of the steady-state heat conduction equation is expressed as [31–34]:

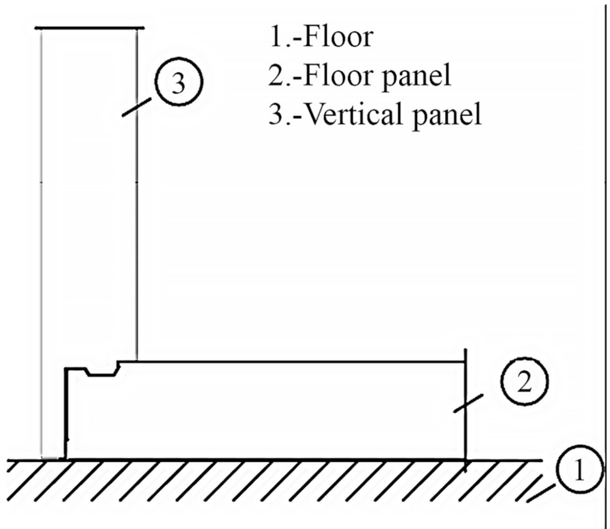


**Fig. 6.** The typical panel-wall-floor joint geometry (reference model) provided in the ETA-10/0376 standard [24].

$$\nabla\cdot(k\nabla T) = 0 \tag{1}$$

Here, $T$ is the temperature field (K), and $k$ is the thermal conductivity (W/m·K), which may be spatially dependent in heterogeneous domains. In Cartesian coordinates, this expands to:

$$\frac{\partial}{\partial x}\left(k\frac{\partial T}{\partial x}\right) + \frac{\partial}{\partial y}\left(k\frac{\partial T}{\partial y}\right) + \frac{\partial}{\partial z}\left(\frac{\partial T}{\partial z}\right) = 0 \tag{2}$$

The heat flux vector $q$ is defined by Fourier's law as:

$$q = -k\nabla T \tag{3}$$

which represents the conductive heat flow rate per unit area. In regions where material interfaces exist (e.g., panel joints), the continuity of both temperature and normal heat flux is enforced:

$$T_1 = T_2, \qquad (k\nabla T)_1 n = (k\nabla T)_2 n \tag{4}$$

where subscripts 1 and 2 refer to adjacent materials and $n$ is the interface normal vector. For numerical implementation via the finite element method (FEM), the weak formulation is derived by applying the weighted residual method. The integral form over the $\Omega$ is given by:

$$\int_\Omega k\nabla T\nabla\omega d\Omega = 0 \tag{5}$$

where $\omega$ is a test function from the same function space as $T$. This formulation allows accurate approximation of temperature fields, particularly in geometrically complex regions such as cold storage panel junctions. Boundary conditions were applied as Dirichlet (fixed temperature) or Neumann (adiabatic or prescribed flux) depending on physical setup. Thermal contact resistance at internal junctions was neglected, assuming ideal contact conditions, consistent with literature practice. In addition to the differential formulation of heat conduction, the steady-state behaviour of thermal systems can be analogized using the concept of thermal resistance, in a manner similar to Ohm's law in electrical systems. In this analogy, the thermal resistance $R_t$ of a material layer is defined as:

$$R_t = \frac{L}{kA} \tag{6}$$

where $L$ is the thickness of the layer (m), $k$ is the thermal conductivity (W/m·K), and $A$ is the cross-sectional area perpendicular to the direction of heat flow (m$^2$). The corresponding heat flux across a layer of material can then be expressed as:

$$q'' = \frac{k}{L}(T_1 - T_2) = \frac{1}{R_t}(T_1 - T_2) \tag{7}$$

This formulation is particularly advantageous for interpreting thermal behaviour across layered systems. In composite wall assemblies, such as multi-jointed insulation panels, the total thermal resistance is computed as the sum of the individual resistances in series:

$$R_{total} = \sum_{i=1}^{n} \frac{L_i}{k_i A} \tag{8}$$

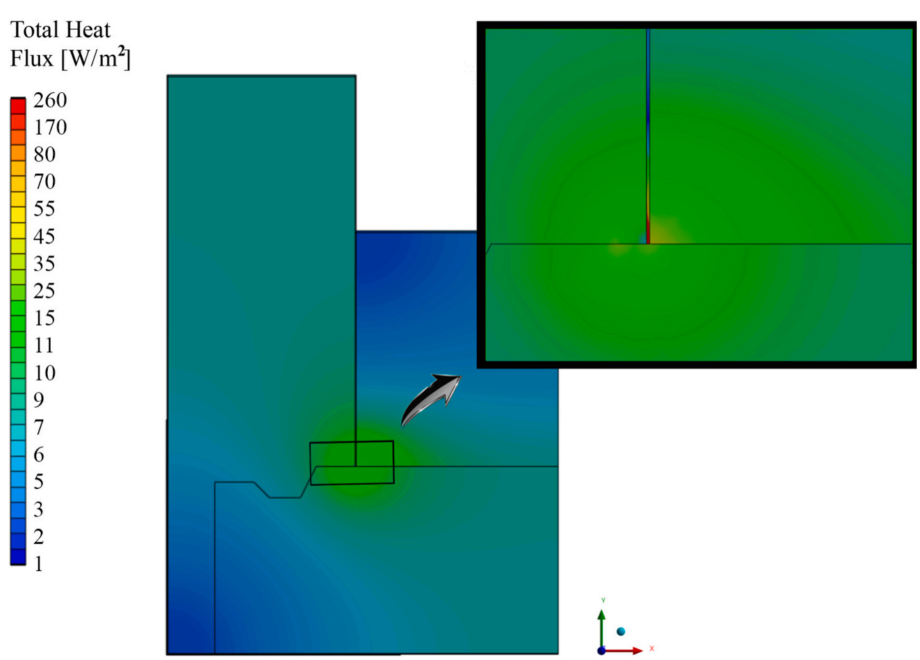


**Fig. 7.** Detailed representation of the local total heat flux concentration formed at the wall–floor junction for reference model, representing the reference junction geometry, under conditions where the internal ambient temperature is 273 K.

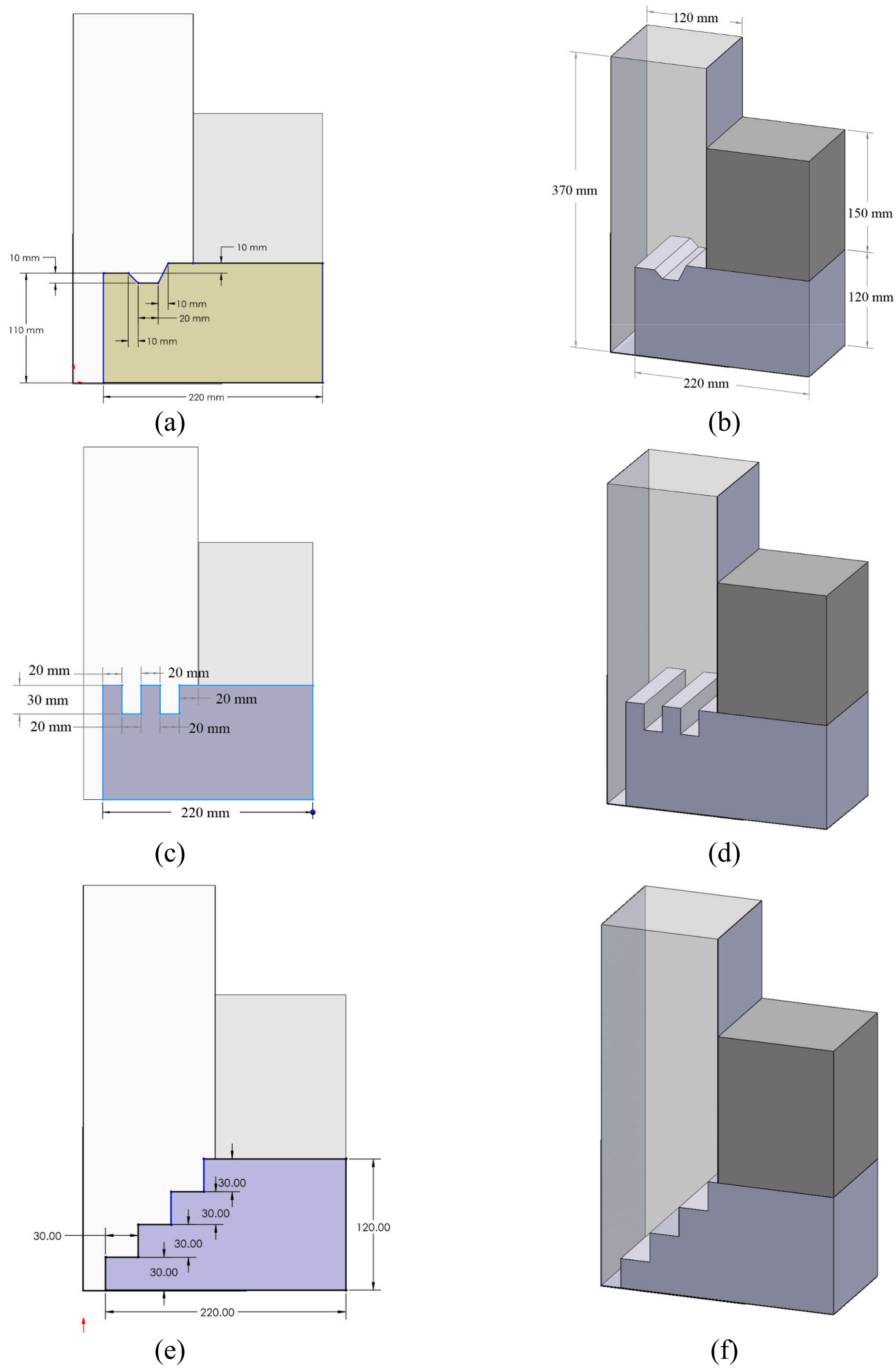


**Fig. 8.** Geometric dimensions of three wall–floor junction configurations (a–b) reference model based on ETA-10/0376 standard geometry [24], (c–d) model 4, (e–f) model 6.

where each layer $i$ may represent a different material in the joint configuration. ANSYS Workbench internally accommodates this resistance-based interpretation when solving one-dimensional conduction problems, whether in planar or cylindrical geometries. This approach enhances both computational efficiency and conceptual clarity, especially in parametric analyses of thermal bridge locations within prefabricated modular cold storage panels.

### 2.4. Model assumptions, boundary and initial conditions

The numerical model employed in this study is formulated under steady-state thermal conditions. Heat transfer within the panel assemblies and joint regions is assumed to occur solely through conduction, while convective and radiative heat transfer effects are not explicitly considered. Moisture transport and humidity-dependent phenomena are not included in the numerical framework; therefore, condensation-related interpretations are limited to indirect assessments based on surface temperature distributions and heat-flux-based indicators.

All materials are assumed to be homogeneous and isotropic, with temperature-independent thermal conductivity values. Perfect thermal contact is assumed at all internal material interfaces, and thermal contact resistance at panel joints is neglected. The geometric configurations are assumed to be ideal, without manufacturing defects, air gaps, or insulation discontinuities beyond those explicitly defined by the joint geometry.

Boundary conditions are prescribed as constant temperatures on the interior and exterior surfaces of the panels, corresponding to the defined indoor temperature scenarios of 255 K and 273 K. Lateral boundaries are treated as adiabatic where appropriate to represent symmetry and to isolate the heat transfer behaviour of the joint region. Since the analysis is conducted under steady-state conditions, the numerical solution is independent of initial conditions.

### 2.5. Dimensionless analysis of normalised temperature and relative heat flux

A unified framework for evaluating thermal performance across different joint configurations was established through the application of two dimensionless parameters: normalised temperature and $q^*$. These quantities enable direct, geometry-independent interpretation of temperature distributions and heat transfer intensity, thereby enhancing the comparability of the numerical results.

#### 2.5.1. Normalised temperature

To facilitate the comparative evaluation of temperature distributions obtained in different panel joint geometries, the numerical results have been rescaled in terms of the normalised temperature parameter ($\theta$). This approach allows temperature variations to be interpreted within a unit interval, independent of the boundary conditions applied in each scenario [33,34].

Normalised temperature is defined as follows:

$$\theta = \frac{T_{model} - T_{model,min}}{T_{model,\ max} - T_{model,min}} \tag{9}$$

Here, $T_{min}$ represents the local temperature, while $T_{max}$ denotes the minimum and maximum temperature values in the calculation area. The temperature fields obtained through this definition are presented in a dimensionless form within the range of 0–1. This allows for a more distinct analysis of local thermal gradients caused by geometric discontinuities.

#### 2.5.2. Relative heat flux ratio

To quantitatively evaluate the thermal bridge effect, the average heat flux values obtained for each joint geometry were dimensionless compared to the reference structure. This approach is an effective metric for directly and comparatively revealing the contribution of joint details to heat transfer. The $q^*$ is defined as follows [32,33]:

$$q^* = \frac{q_{model}}{q_{ref}} \tag{10}$$

Here, the $q^*$ denotes the average heat flux density determined in the examined structure configuration, while $q_0$ denotes the corresponding value obtained in the flat-contact reference joint. $q_{model}$ is the calculated average heat flux of the relevant model, and the heat flux of the reference model is generally the highest ($q_{max}$ ) which is selected because it has the worst insulation performance and the others are compared to it. This ratio numerically represents the additional heat losses caused by geometric discontinuities. A value above 1 indicates greater heat loss compared to the reference structure, while a value below 1 indicates better insulation performance. This dimensionless parameter enables the systematic comparison of different joint designs in terms of energy performance. Thus, the effect of thermal bridges can be examined.

### 2.6. Physical interpretation and relation to standard indicators

The dimensionless parameters used in this study are defined to enable both local and comparative interpretation of the thermal bridge behaviour associated with joint geometries. $\boldsymbol{\theta}$, renders the temperature field within the joint region independent of absolute temperature levels, thereby allowing direct comparison of local temperature distributions induced by different geometries. This parameter represents the intensity of thermal gradients formed within the joint region and the degree of temperature field homogeneity, and more uniform distributions have been examined as indicative of a more balanced heat transfer behaviour.

$\boldsymbol{q^*}$, is a dimensionless indicator that quantitatively expresses the heat transfer behaviour of a given joint geometry relative to a reference configuration. This parameter reflects the extent to which the joint geometry alters the conductive heat transfer path, thereby directly revealing the influence of geometric discontinuities on the formation of thermal short-circuits. Relative heat flux ratios greater than unity indicate a more intense heat flux compared to the reference case and, consequently, a more pronounced thermal bridge effect, whereas values below unity indicate that the geometric arrangement is effective in reducing heat loss.

In this study, the use of dimensionless parameters enables the local distribution of heat transfer within the joint region to be examined in a geometry-oriented and comparative manner. This approach allows consistent evaluation of the thermal bridge behaviour of different joint configurations, through which the physical implications of geometric discontinuities on local heat transfer mechanisms have been assessed.

## 3. Results and discussion

### 3.1. Temperature field distributions and thermal bridging characteristics

The temperature field distributions of different joint geometries were examined, and their effects on thermal bridge formation were evaluated in a comparative manner. Fig. 9 shows the temperature distribution contours for six different joint models when the internal environment temperature is set to 273 K. Similar to the findings obtained at 255 K, Model 1 (flat-contact joint) exhibits a steep and intensely localized temperature gradient along the joint line, clearly revealing the direct heat transfer path. This confirms the inadequacy of this joint structure in preventing thermal bridging, particularly in scenarios where ambient temperatures are higher and heat input becomes more pronounced.

Model 2 (*Z*-joint), thanks to its single-step geometry, creates a thermal barrier that partially interrupts the conduction path, thereby limiting heat diffusion towards the interior volume to some extent. However, the low-temperature regions formed near the recessed corners in the joint area indicate that local heat conduction is still effective.

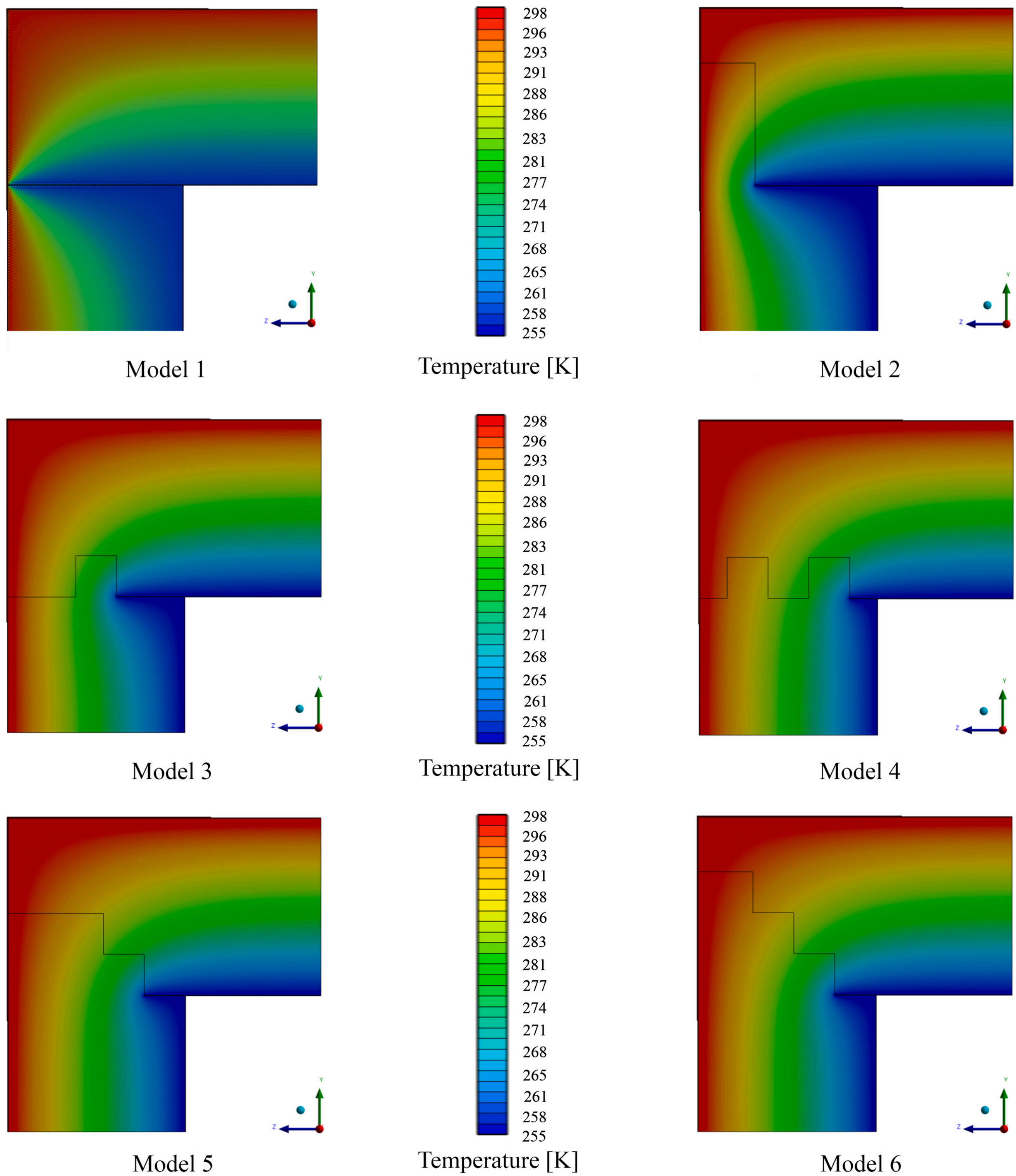


**Fig. 9.** Temperature contour distributions of six different joint configurations under an internal temperature of 255 K.

Model 3 (single-stage overlapping joint) and Model 4 (double-stage overlapping joint) extend the heat transfer path, allowing the thermal load to be spread over larger surfaces. Particularly in Model 4, the presence of multiple contact surfaces ensures a more homogeneous distribution of the temperature gradient and reduces the thermal intensity at the interface more than Model 3. Model 5 (two-stage interlocking joint) and Model 6 (multi-stage interlocking joint), on the other hand, significantly extend the heat transfer path thanks to their multi-layered and interlocking geometric designs, thereby maximising insulation integrity. In these configurations, the temperature field becomes progressively smoother and more homogeneous, with Model 6 in particular offering superior insulation performance by exhibiting minimal thermal leakage along the joint line. These findings clearly demonstrate the advantages of complex interlocking structures in suppressing thermal bridge effects under moderate cooling conditions. Furthermore, it confirms that the joint geometry plays a critical role in maintaining cold room thermal integrity not only at low temperatures but also under near-zero temperature conditions. This analysis, conducted under low-temperature conditions (255 K), allows thermal bridge effects to emerge earlier and more distinctly. This facilitates the visual tracking of weak points in insulation continuity and surface temperature differences. Furthermore, this temperature level is a value frequently encountered in commercial cold room applications and is considered representative for evaluating the behaviour of panel joint performance under critical thermal scenarios. Therefore, conducting temperature contour analyses below 255 K has formed the basis for comparative thermal performance analysis between configurations. Although the average surface temperatures obtained for different joint geometries remain within a relatively narrow range, the corresponding heat flux values exhibit pronounced variations. This clearly indicates that surface temperature alone is insufficient to reliably characterize thermal bridge severity, whereas heat flux provides a more sensitive and geometry-dependent indicator.

### 3.2. *Heat flux vector analysis and directional conductivity characteristics*

The orientation of heat flux vectors enables the thermal behaviour of composite structures to be examined in a level of detail that cannot be obtained solely from temperature contours. By examining the vector distributions obtained at an internal ambient temperature of 273 K, it is possible to evaluate how each composite geometry directs or concentrates heat flux. These directional analyses enable the detection of local heat bridge formations and reveal the effectiveness of step or transition structures in distributing conductive loads. Minimising directional heat leakage is particularly critical for long-term insulation efficiency in modular cold room systems.

Fig. 10 presents the heat flux vector distributions for each joint model in a scenario where the internal ambient temperature is set at 273 K. These vector visualisations reveal both the direction of heat transfer and the local transfer intensity, enabling a qualitative assessment of the joint geometry's effect on thermal bridge formation. Model 1 (Flat butt joint) exhibits a strong thermal bridge effect, with heat flux being transferred linearly and intensely into the interior volume. The vectors in this structure pass through the joint plane with minimal resistance and are directed directly into the interior volume. Model 2 (*Z*-joint), with its single-step structure, causes the heat flow to change direction to a certain extent; however, localized concentrations are still observed at the inner edge corners. Models 3 and 4 (single and double overlap structures) spread the heat over wider surfaces, thereby increasing thermal conduction and reducing temperature differences in the joint

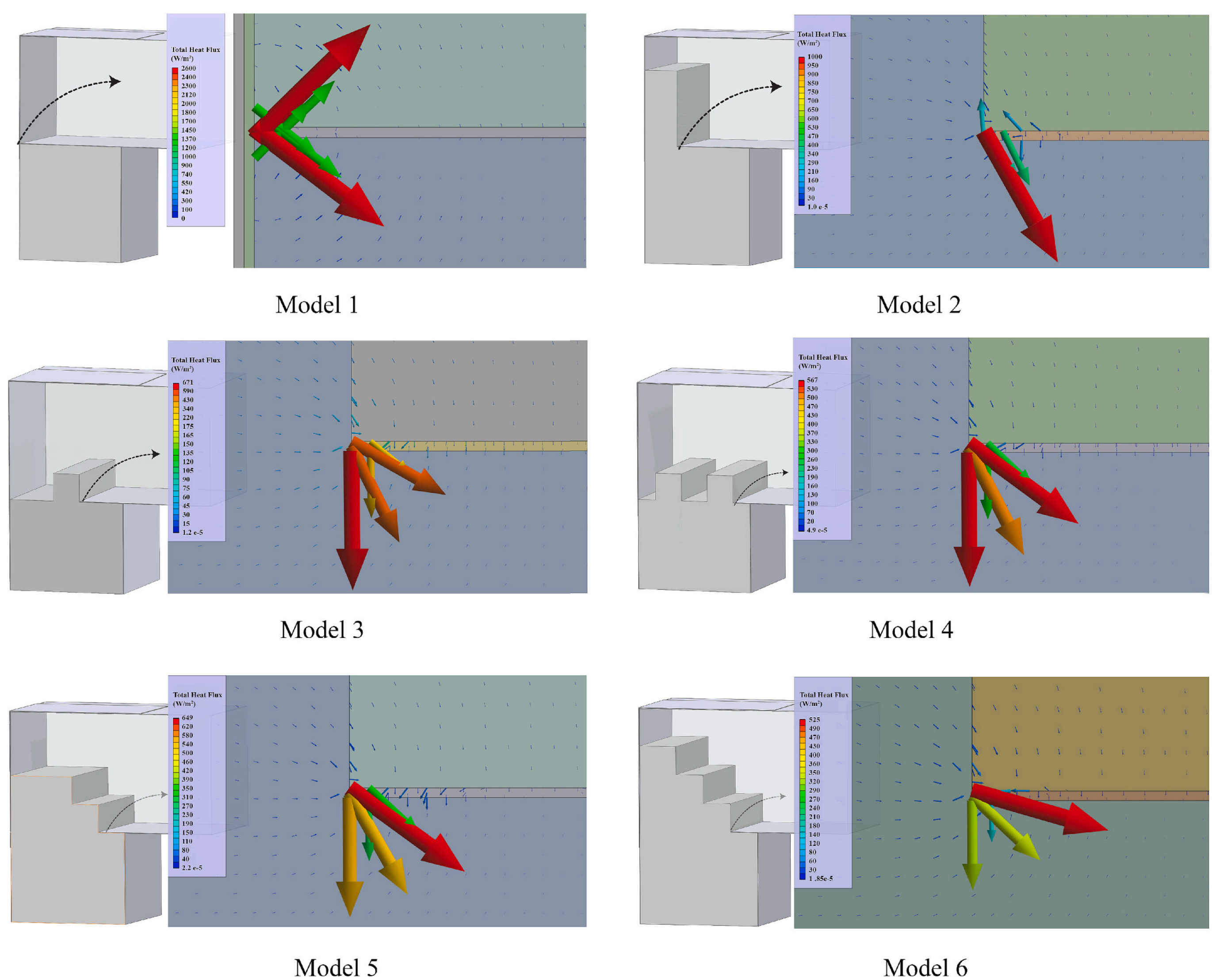


**Fig. 10.** Directional and magnitude distribution of heat flux vectors for six different joint models under an internal setpoint temperature of 273 K.

area.

In Model 4 in particular, multiple contact surfaces ensure a more uniform heat flow. Model 5 (Double-step interlocking joint) and Model 6 (Multi-step interlocking joint) increase thermal resistance and limit heat transfer by directing the heat flow into the interior volume through broken paths. Model 6, in particular, minimises the thermal bridge effect with directionally broken low-density flux vectors. This analysis demonstrates that the joint geometry affects not only temperature fields but also heat flux direction. Complex interlocking structures offer significant advantages in enhancing interior insulation efficiency. The primary reason for choosing 273 K as the internal ambient temperature in this analysis is to more clearly visualise the directional deviations and magnitude differences of the heat flux vectors. At low temperatures (e.g., 255 K), heat conduction rates are limited, reducing the interpretability of vector distributions and causing the effect of fine geometric details to fade into the background. In contrast, at 273 K, the directing effect of the junction geometry on heat flow becomes more pronounced; thermal short circuits and directional leaks can be identified more reliably. Therefore, heat flux vector analyses were performed at a temperature of 273 K, and all configurations were compared in this context.

### 3.3. Comparative evaluation with standard joint designs

The standards prEN 14509-1 and prEN 14509-2 [24,35,36], which are planned to be published soon alongside ETA 10/0376 within the current regulatory framework, define the basic requirements for the structural and thermal performance of prefabricated sandwich panels. While these standards contain general rules regarding panel materials, mechanical strength conditions, and declared thermal conductivity coefficients, they do not provide specific guidance on thermal bridge formation in joint areas. Within this context, the present study focuses on the influence of joint geometry on local heat flux paths and temperature gradients through high-resolution numerical analyses, providing additional insight into thermal bridge behaviour at panel joints.

Fig. 11 presents a comparative analysis of the average surface temperature and heat flux values for six different junction models, with the ambient temperature set at 273 K. Model 1 with a flat joint geometry and Model 2 with a Z-type transition exhibited the lowest surface temperatures of 285.96 K and 286.51 K, respectively; at the same time, they reached the highest heat flux values of 9.87 W/m$^2$ and 10.06 W/m$^2$. This indicates that thermal short-circuit effects are dominant along the joint line in these two models, and heat bridge formation is pronounced.

In contrast, Models 4 and 6, which have a multi-step transition structure, stand out with high surface temperatures of 288.93 K and 288.62 K; accompanied by low heat flux values of 7.46 W/m$^2$ and 7.61 W/m$^2$, indicating better insulation performance. This situation shows that thermal bridge formation is limited and heat transfer in the joint region is minimised. Interlocking structures, which redirect the escaping heat flux by increasing geometric complexity, have made it possible to control heat losses at critical joint points. When evaluated in terms of condensation risk, the fact that all surface temperatures remain above the dew point temperature (~273 K, 100% relative humidity) under indoor conditions of 273 K indicates that the possibility of vapour condensation is reduced. Particularly in Model 4 and Model 6, the higher level of surface temperature maintenance prevents vapour condensation from occurring on the inner surface, thereby preventing moisture-related structural deterioration. Therefore, Models 4 and 6 clearly demonstrate that optimised interlocking joint geometries offer superior performance compared to traditional joint details in terms of both heat loss reduction and condensation risk limitation. The preference for these structures is increasing in terms of energy efficiency and the sustainability of indoor environmental quality. Despite comparable surface temperature levels, significant differences in heat flux magnitude are observed among the joint configurations.

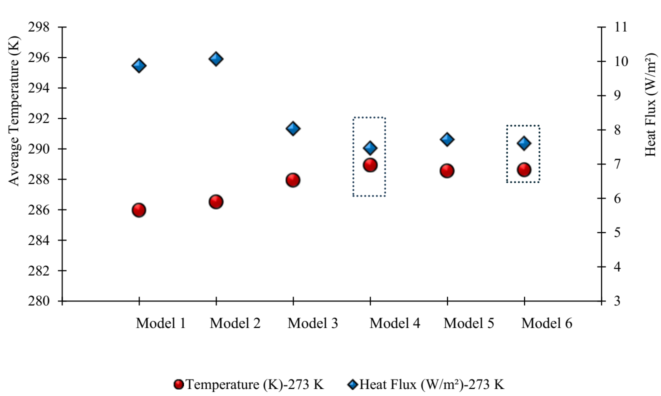


**Fig. 11.** Comparative evaluation of temperature and heat flux values under 273 K indoor temperature.

Fig. 12 presents a comparative analysis of the average surface temperature and heat flux values for six different composite models under conditions where the indoor ambient temperature is defined as 255 K. High heat flux values and low surface temperatures are particularly evident for Model 1 (17.04 W/m$^2$, 277.1 K) and Model 2 (17.31 W/m$^2$, 278.13 K), indicating significant heat loss and thermal discontinuity in the joint areas of these structures. This situation indicates that, despite the adiabatic external wall boundary conditions, energy transfer from the internal environment to the external environment is increased due to insufficient insulation. In contrast, Model 4 and Model 6 have the lowest heat flux values (12.83 W/m$^2$ and 13.08 W/m$^2$, respectively) and demonstrate the best insulation performance with high average surface temperatures of 282.29 K and 281.75 K. Model 4, in particular, stands out with both the lowest heat loss and the highest surface temperature, demonstrating that it offers an optimal joint geometry in terms of preventing heat bridge formation in cold room applications. When evaluated in terms of condensation risk, configurations such as Model 1 and Model 2, which have low surface temperatures, have values closer to the dew point under the assumption of 100% relative humidity in the indoor environment. Therefore, the potential for condensation is higher in the joint areas of these models. In contrast, the high surface temperatures observed in Model 4 and Model 6 allow vapour to remain on the surface without condensing, providing an advantage in terms of humidity management.

Table 2 presents a comparative analysis of the average surface temperatures and heat flux values for six composite models under two different scenarios where the indoor temperatures are set at 255 K and 273 K. This evaluation aims to analyze the thermal insulation performance of the models under both low and high indoor temperature conditions. Model 1, with a flat joint, exhibits the highest heat flux values (255 K: 1266 W/m$^2$, 273 K: 2276 W/m$^2$) at both temperature levels, demonstrating the weakest insulation performance. Similarly, critically high heat flux was observed in Model 2 with a Z-type structure, indicating that the model is susceptible to thermal bridging and that its insulation capability is severely limited. Model 3 has balanced average surface temperatures and a significant decrease in heat flux values compared to Models 1 and 2 (255 K: 0.682 W/m$^2$, 273 K: 1.402 W/m$^2$). This structure provides a medium level of insulation performance. The most successful performance was achieved in Model 4 and Model 6, where multi-step interlocking structures were applied. Both models showed the lowest heat flux values in all scenarios (Model 4–255 K: 0.390 W/m$^2$, 273 K: 0.865 W/m$^2$; Model 6–255 K: 0.415 W/m$^2$, 273 K: 0.868 W/m$^2$), indicating effective thermal insulation. Furthermore, Model 6 stands out with values similar to Model 4, demonstrating that it can successfully maintain insulation continuity. Model 5, on the other hand, has demonstrated good insulation performance with low heat flux and high average surface temperature; it is understood that this model has also been improved, particularly from a design perspective. Therefore, in terms of limiting heat flux and increasing internal surface temperatures, Models 4 and 6 stand out as the models providing the highest

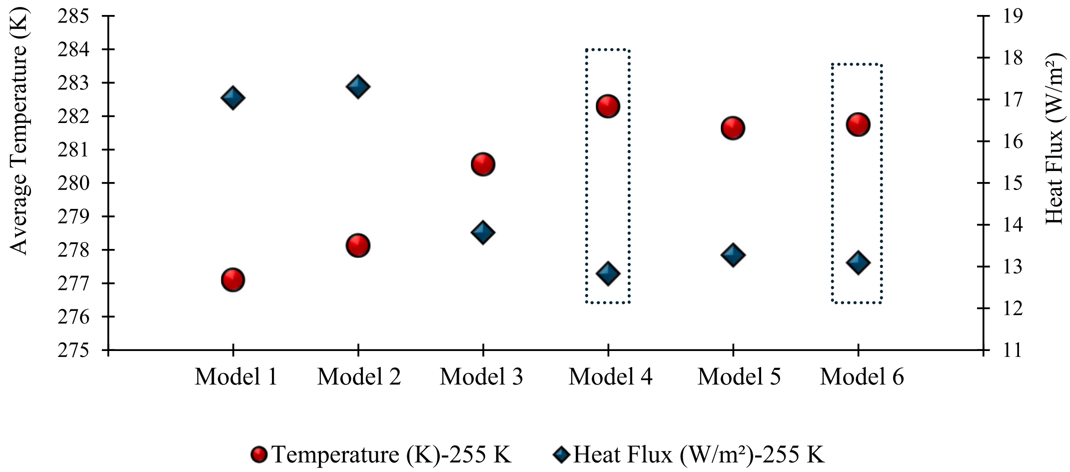


**Fig. 12.** Comparative evaluation of temperature and heat flux values under 255 K indoor.

**Table 2**
Comparative thermal performance and heat flux evaluations of joint models at 255 K and 273 K internal temperatures.

| Model | Avg. Surface Temp. (255 K) | Avg. Surface Temp. (273 K) | Heat Flux (W/m$^2$)-255 K | Heat Flux (W/m$^2$)-273 K | Thermal Performance | Heat Flux Evaluation |
|---|---|---|---|---|---|---|
| 1 | 283.92 | 289.47 | 1.266 | 2.276 | Poor insulation | High heat flux at both temperatures → Poor insulation |
| 2 | 284.53 | 289.99 | 1.117 | 2.010 | Poor insulation | Critical heat flux values → Severely limited insulation |
| 3 | 286.61 | 291.38 | 0.682 | 1.402 | Moderate insulation | Noticeably reduced flux → Moderate insulation |
| 4 | 288.78 | 292.85 | 0.390 | 0.865 | Highly effective insulation | Lowest flux observed → Highly effective insulation |
| 5 | 287.60 | 291.97 | 0.509 | 1.021 | Good insulation | Low and stable flux → Enhanced insulation performance |
| 6 | 288.16 | 292.40 | 0.415 | 0.868 | Highly effective insulation | Comparable to Model 4 → Highly effective insulation |

insulation efficiency in both temperature scenarios. Compared to other models, these structures offer optimised composite designs in terms of reducing heat loss and minimising condensation risk.

### *3.4. Evaluation of dimensionless thermal field characteristics*

Fig. 13 presents the results obtained at reference temperatures of 255 K and 273 K for six different model configurations, with values presented comparatively. The fact that the profiles obtained under both temperature scenarios show very similar trends indicates that the thermal performance of the analysed geometric structures exhibits an insensitive character to the inlet temperature. This is important in that it shows that the thermal stability of the designed models can be maintained under different external environmental conditions.

The results obtained for Model 4 and Model 6 stand out with their low and horizontal values in both scenarios. The low relative heat flux indicates that heat transfer is minimal in these areas, thus reducing heat

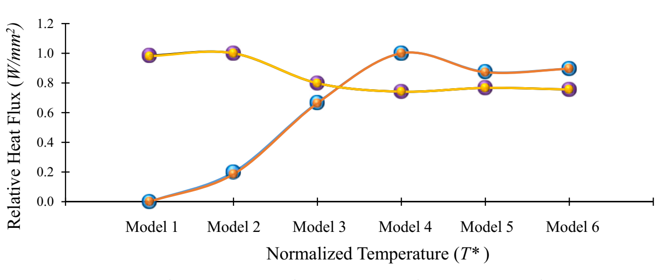


**Fig. 13.** Variation of $T^*$ and $q^*$ for different models of 255 K and 273 K.

leakage and providing effective insulation. In these models, the tendency of normalised temperature values to approach →1 also indicates that the temperature difference is minimised and the temperature distribution on the surface is balanced, which can be said to limit the formation of thermal bridges. Furthermore, as the values approach 1, the values also approach zero, indicating not only that the surface temperatures have become homogeneous, but also that the heat flow in these areas has been reduced to a negligible level. The simultaneous attainment of ideal values for these two dimensionless parameters clearly demonstrates that the relevant structural components both suppress heat transfer through conduction and exhibit superior performance in terms of thermal continuity. These findings confirm that Model 4 and Model 6 provide better thermal continuity in the building envelope, suppress heat transfer, and exhibit a homogeneous distribution of temperature gradients. Consequently, this analysis using normalised dimensionless parameters strongly highlights not only the temperature field but also the effect of geometric variations on systematic heat loss, providing a robust engineering criterion for model comparisons.

### *3.5. Wall-floor junction thermal bridges*

The thermal behaviour of wall-floor junctions has been examined based on numerical results obtained for reference and improved geometric configurations. Evaluations were carried out based on temperature fields and heat flux distributions. Fig. 14 presents the temperature distribution contours for three configurations developed for the wall-floor joint at an internal ambient temperature of 273.15 K. Fig. 14(a) serves as a reference based on the rotary hook locking geometry in the ETA-10/0376 standard, exhibiting a distinct thermal gradient ($\Delta T \approx 10$ K) and a pronounced thermal bridge effect along the joint line. Fig. 14(b)

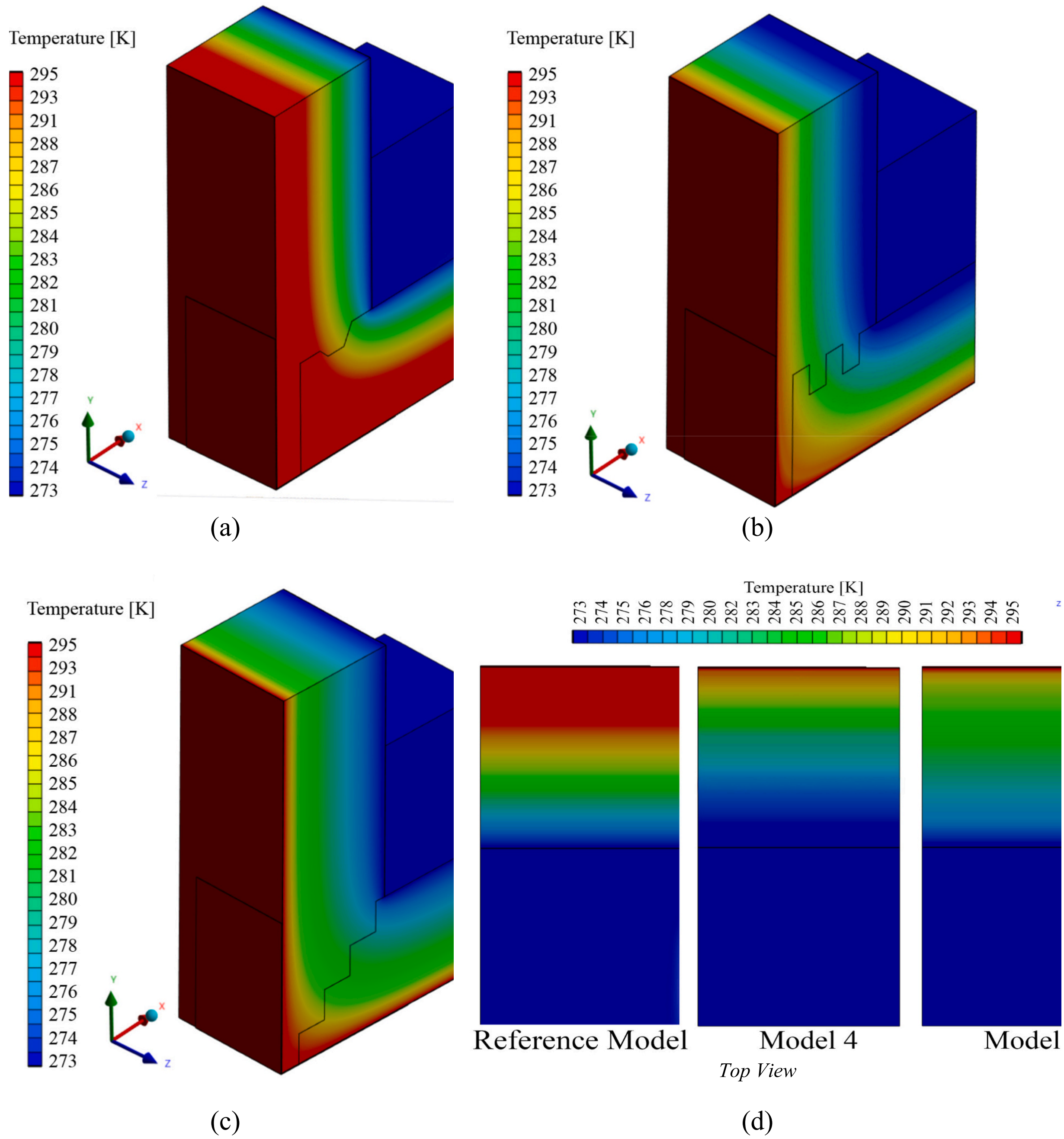


**Fig. 14.** Temperature distribution contours at an internal ambient temperature of 273.15 K in wall-floor junction configurations: a) reference model, b) model 4, c) model 6 d).

homogenises the gradient (ΔT ≈ 6 K) by extending the transmission path with a double-step overlap; Model 6 (Fig. 14c) achieves the lowest local cold spot density at ΔT ≈ 4 K and maximises insulation continuity through multi-step overlap. These contours demonstrate that stepped geometries systematically reduce the thermal bridge effect.

In assessing the thermal bridge effect at wall-floor junctions, average surface temperatures do not provide a distinctive performance metric, as they typically vary within a limited range. In contrast, heat flux density is the fundamental physical quantity that directly reflects the extent to which the junction geometry shortens or lengthens the conduction path. Therefore, the thermal performance of these junctions was evaluated in this study based on heat flux rather than temperature levels. Changes in heat flux reveal the degree of insulation continuity disruption and local thermal bridge behaviour more accurately, and the effectiveness of geometric improvements can be directly monitored through this parameter. Fig. 15 shows the average surface temperature and heat flux values for Reference model, Model 4, and Model 6 configurations examined for the wall-floor joint at an internal ambient temperature of 273.15 K. The heat flux values show significant differences between the models. Reference model, representing the reference geometry, produces the highest heat flux at approximately 6.7 W/m$^2$; in the double-stepped overlapping Model 4, this value drops to ≈6.6 W/m$^2$, and in the multi-stepped interlocking Model 6, it reaches a minimum level of ≈6.5 W/m$^2$. These results show that, although the composite geometry has a limited effect on surface temperature, it significantly reduces heat flux by extending and directing the heat transfer path.

Fig. 16 presents the temperature distribution contours for three different configurations examined for the wall–floor junction at a

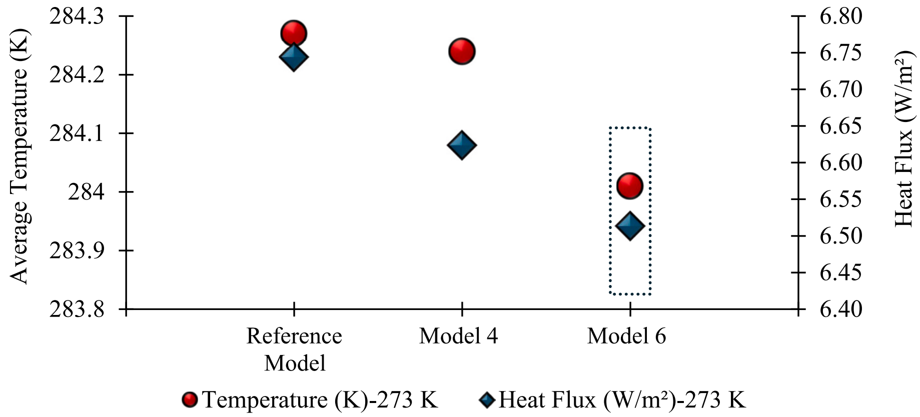


**Fig. 15.** Comparison of average surface temperature and average heat flux values at 273.15 K in wall-floor junction configurations.

storage interior temperature of 255 K. Although similar surface temperature ranges are observed in all models at low temperature levels, it is seen that the isotherms concentrate in different ways along the joint line depending on the joint geometry. In Reference model, representing the reference geometry, the sharp compression of the isotherms in the joint region indicates a strong conduction path and pronounced thermal bridge behaviour. In the stepped-overlap Model 4, the isotherms exhibit a more diffuse distribution, indicating an elongated conduction path; in the multi-step-overlap Model 6, the fractured and stepped isotherm structure reveals that heat conduction changes direction and effective thermal resistance increases in the junction region. These observations confirm that, under critical operating conditions such as −18 °C, thermal bridge behaviour is shaped more by how the geometry directs the heat transfer path than by the temperature level.

Fig. 17 presents the average heat flux and surface temperature values for reference model, Model 4, and Model 6 configurations examined for the wall–floor junction under conditions where the indoor ambient temperature is 255 K. At this temperature level, the average surface temperatures for all models' cluster within a very close range, and it is understood that the temperature differences provide limited information for distinguishing thermal bridge behaviour. In contrast, the heat flux values are directly sensitive to joint geometry and show significant differences between models. Reference model, representing the reference geometry, has the highest heat flux at approximately 12.6 W/m$^2$, while this value drops to ≈12.3 W/m$^2$ in the stepped overlapping Model

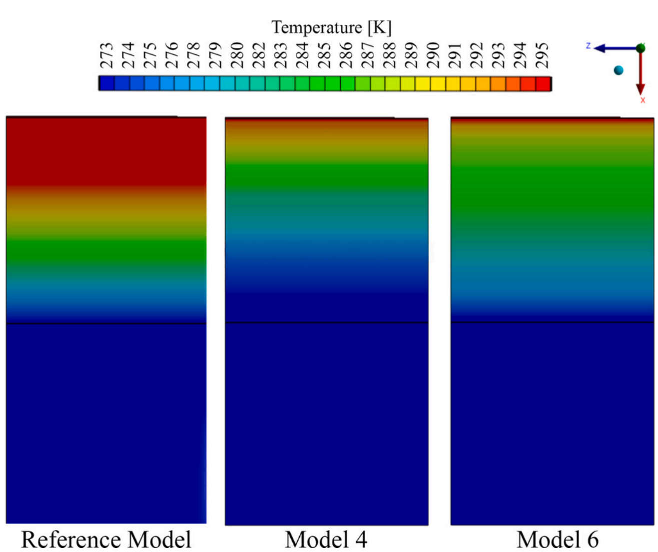


**Fig. 16.** 255 K temperature distribution contours for the wall–floor junction at indoor temperature.

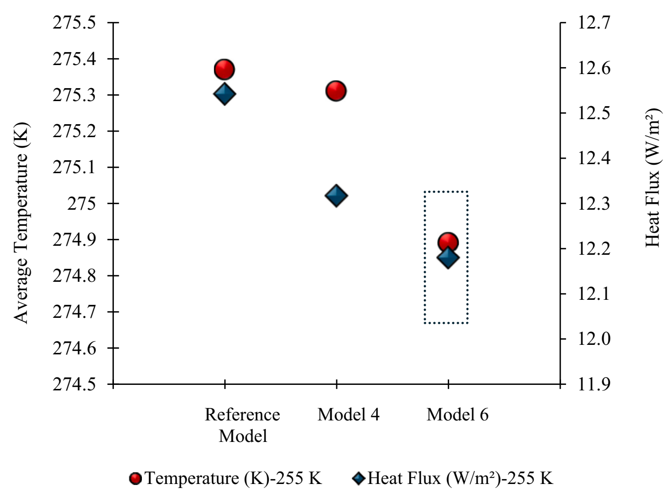


**Fig. 17.** Comparison of average surface temperature and average heat flux values for wall–floor junctions at an indoor temperature of 255 K.

4 and reaches a minimum of ≈12.2 W/m$^2$ in the multi-stepped overlapping Model 6. This trend demonstrates that, at low indoor temperatures, evaluating the thermal bridge effect based on heat flux density rather than surface temperatures is more accurate and distinctive; it confirms that the joint geometry effectively limits heat loss by extending the conduction path.

To enable a quantitative comparison of thermal bridge behaviour in joint regions, normalising the absolute heat flux values relative to a reference configuration is a common and physically meaningful approach. In this context, the relative heat flux is defined as the ratio of the average heat flux obtained in each joint geometry to the heat flux of the reference model defined under the same boundary conditions. As a dimensionless quantity, $q^*$ allows for a direct and scale-independent comparison of the thermal bridge severity of different geometries.The relative heat flux values presented in Fig. 18(a) enable the thermal bridge behaviour of the joint geometries to be quantitatively evaluated relative to the reference model. For Reference model, representing the reference configuration, the $q^*$ value is equal to the unit value, and the other models are normalised relative to this value. In the stepped overlapping Model 4, the $q^*$ value falls below the unit value under both temperature conditions, indicating that the joint geometry limits the thermal bridge effect by extending the heat transfer path. The multi-stepped overlapping Model 6 exhibits the lowest $q^*$ values, providing the most effective thermal improvement compared to the reference configuration. Furthermore, the fact that the $q^*$ curves obtained for 255 K and 273 K are quite close to each other reveals that the relative heat

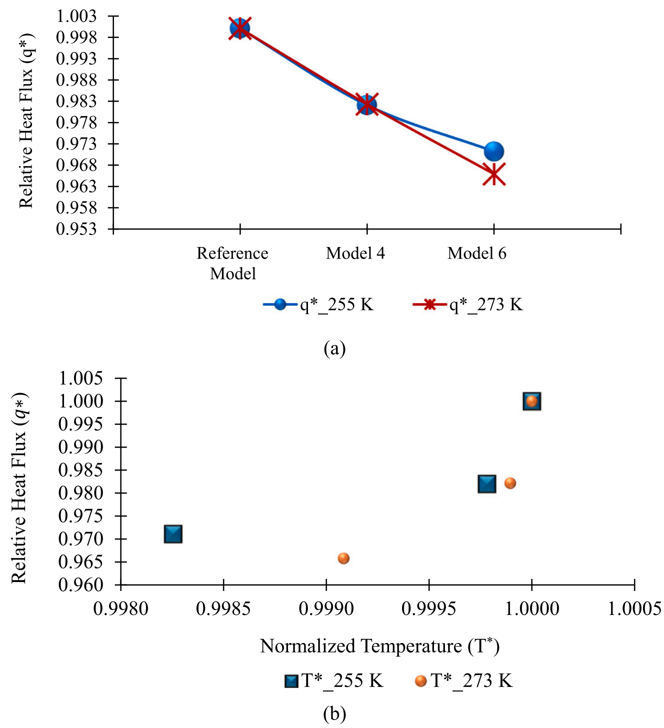


**Fig. 18.** Comparison of a) $q^*$ values for wall–floor junctions at indoor temperatures of 255 K and 273 K b) the relationship between $T^*$ and $q^*$.

flux is largely independent of the temperature level and that the geometric effect plays a dominant role. Fig. 18 (b) shows the relationship between the normalised surface temperature ($T^*$) and the $q^*$. Although the $T^*$ values are very close to unity for all joint geometries, the $q^*$ values are seen to differ significantly. This clearly demonstrates that surface temperature is limited in distinguishing thermal bridge severity, whereas heat flux density provides a metric that is sensitive to joint geometry and more discriminating.

## 4. Conclusion

In this study, the effect of different joint geometries on the thermal bridge behaviour of prefabricated modular cold room panels was systematically investigated through high-resolution numerical analyses, experimentally validated. The analyses were performed for wall–wall, wall–ceiling, and particularly wall–floor joints at internal ambient temperatures of 255 K and 273 K; the results were evaluated in terms of temperature fields, heat flux vectors, and dimensionless performance parameters. The results clearly demonstrate that the joint geometry plays a decisive role in the formation of thermal bridges. It was observed that flat-contact and simple Z-type joints create short and direct transmission paths along the joint line, leading to high local heat flux intensities. In contrast, it was determined that stepped overlapping and multi-step interlocking joint geometries effectively limit heat transfer by extending the conduction path and changing its direction. This effect was consistently observed in both absolute heat flux values and the $q^*$ parameter, particularly in Model 4 and Model 6 configurations.

The results indicate that surface temperatures exhibit only minor variations among the investigated joint geometries, whereas heat flux values differ markedly between the models. Accordingly, the findings confirm that thermal bridge assessment based solely on surface temperature may lead to misleading interpretations, while heat-flux-based metrics offer a more robust evaluation framework. This situation demonstrates that approaches based solely on surface temperatures are insufficient for evaluating thermal bridge severity; in contrast, heat flux density and relative heat flux provide a performance metric that is sensitive to the joint geometry and more discriminating. The relationship between $T^*$ and $q^*$ confirms that thermal bridge behaviour is largely independent of the temperature level and is determined by geometric discontinuities.

The analyses presented in this study are based on steady-state thermal conditions. Within this framework, long-term performance is not addressed through time-dependent modelling, but rather interpreted using time-independent physical indicators such as heat flux intensity, extended heat transfer paths, and the tendency for thermal short-circuit formation. The steady-state results enable an assessment of how these indicators are influenced by joint geometry. In this context, the findings allow a qualitative evaluation of the trends that geometric improvements may induce in long-term thermal behaviour [37].

Analyses specific to wall–floor junctions revealed that this interface is one of the most critical thermal bridge areas in prefabricated cold room systems. In the reference junction geometry based on the ETA-10/0376 standard, a pronounced local heat flux concentration and dominant thermal short-circuit behaviour were observed. In contrast, adapting validated stepped and interlocking designs from wall-ceiling joints to floor joints reduced heat flux intensity and increased insulation continuity. This finding demonstrates that existing standard joint details can be thermally improved with advanced geometric designs. This study demonstrates that evaluating thermal bridges in prefabricated cold room panels using heat flux-based and dimensionless metrics rather than temperature-based indicators provides a more accurate and reliable approach. The findings indicate that joint details, which are not sufficiently addressed in current standards, are critical in terms of energy efficiency and reducing the risk of condensation. The study results are expected to provide an engineering-based reference for future standard revisions and the development of cold room joint designs.

## CRediT authorship contribution statement

**Gulenay Alevay Kilic:** Writing – review & editing, Writing – original draft, Visualization, Validation, Supervision, Software, Project administration, Methodology, Investigation, Formal analysis, Data curation, Conceptualization. **Enver Yalcin:** Writing – review & editing, Visualization, Validation, Methodology, Data curation, Conceptualization.

## Declaration of Generative AI and AI-assisted technologies in the writing process

During the preparation of this work, the author(s) used generative AI tools for language improvement. After using these tools, the author(s) reviewed the content as needed and take(s) full responsibility for the content of the published article.

## Declaration of competing interest

The authors declare that they have no known competing financial interests or personal relationships that could have appeared to influence the work reported in this paper.

## Data availability

Data will be made available on request.

## References

[1] The Agreement on the International Carriage of Perishable Foodstuffs and on the Special Equipment to be Used for such Carriage (ATP), United Nations, 2014. http://www.unece.org/fileadmin/DAM/trans/doc/2014/wp11/ATP-2014_E.pdf (accessed December 2014).

[2] Turkish Standards Institution, TR EN ISO 10211 Thermal bridges in building construction Heat flows and surface temperatures - Detailed calculations. https://www.iso.org/obp/ui/en/#iso:std:iso:10211:ed-2:v1:en, April 2009.

[3] S.A. Al-Sanea, M.F. Zedan, Effect of thermal bridges on transmission loads and thermal resistance of building walls under dynamic conditions, Appl. Energy 98 (2012) 584–593, https://doi.org/10.1016/j.apenergy.2012.04.038.

[4] A.F. BrásGonçalves, P. Faustino, Cork-based mortars for thermal bridges correction in a dwelling: Thermal performance and cost evaluation, Energ. Buildings 72 (2014) 296–308, https://doi.org/10.1016/j.enbuild.2013.12.022.

[5] K. Karabulut, E. Buyruk, A. Fertelli, Numerical investigation of heat transfer for thermal bridges according to change of outside environment temperature, Cukurova Univ. J. Facult. Eng. Architect. 26 (2) (2011) 87–97.

[6] C. Bekler, İ. Ayçam, M.Z. Yılmazoğlu, Analysis of thermal performance of an innovative thermal storage wall, J. Build. Eng. 103 (2025) 112058, https://doi.org/10.1016/j.jobe.2025.112058.

[7] M. Khoukhi, A. Hassan, S. Al Saadi, S. Abdelbaqi, A dynamic thermal response on thermal conductivity at different temperature and moisture levels of EPS insulation, Case Stud. Therm. Eng. 14 (2019) 100481, https://doi.org/10.1016/j.csite.2019.100481.

[8] A. Güner, Ş. Dilmaç, M.T. Cihan, ISO 9164 heat loss in roof-wall sections, Sci. Res. Essays 6 (20) (2011) 4354–4368. http://www.academicjournals.org/SRE.

[9] T. Theodosiou, K. Tsikaloudaki, K. Kontoleon, C. Giarma, Assessing the accuracy of predictive thermal bridge heat flow methodologies, Renew. Sust. Energ. Rev. 136 (2021) 110437, https://doi.org/10.1016/j.rser.2020.110437.

[10] J.A. Paz-Pérez, R.E. López-Guerrero, M. Carpio, Evaluating the impact of thermal bridges on the thermal performance of concrete and mass timber buildings: case study in Chile, Case Stud. Therm. Eng. (2025) 107014, https://doi.org/10.1016/j.csite.2025.107014.

[11] P. Lisowski, M.A. Glinicki, Promising biomass waste–derived insulation materials for application in construction and buildings, Biomass Convers. Biorefinery 15 (1) (2025) 57–74, https://doi.org/10.1007/s13399-023-05192-8.

[12] P. Sokołowski, T. Jakubowski, G. Nawalany, A. Atilgan, S. Syrotyuk, Numerical analysis of the effect of floor depression on the extent of thermal interaction with the ground and energy management using a vegetable cold store as an example, Energies 17 (2023) 5, https://doi.org/10.3390/en17010005.

[13] A. Sepehri, G.S. Pavlak, Evaluating optimal control of active insulation and HVAC systems in residential buildings, Energ. Buildings 281 (2023) 112728, https://doi.org/10.1016/j.enbuild.2022.112728.

[14] K. Martin, A. Erkoreka, I. Flores, M. Odriozola, J.M. Sala, Problems in the calculation of thermal bridges in dynamic conditions, Energ. Buildings 43 (2011) 529–535, https://doi.org/10.1016/j.enbuild.2010.10.018.

[15] G. Wang, J. Fang, C. Yan, D. Huang, K. Hu, K. Zhou, Advancements in smart building envelopes: a comprehensive review, Energ. Buildings 312 (2024) 114190, https://doi.org/10.1016/j.enbuild.2024.114190.

[16] A. El Saied, C. Maalouf, T. Bejat, E. Wurtz, Slab-on-grade thermal bridges: a thermal behavior and solution review, Energ. Buildings 257 (2022) 111770, https://doi.org/10.1016/j.enbuild.2021.111770.

[17] J. Ge, Y. Xue, Y. Fan, Methods for evaluating and improving thermal performance of wall-to-floor thermal bridges, Energ. Buildings 231 (2021) 110565, https://doi.org/10.1016/j.enbuild.2018.03.044.

[18] Y. Xue, K. Zhao, Y. Qian, J. Ge, Improved operating strategy for air-conditioning systems based on the indoor occupancy rate, J. Build. Eng. 29 (2020) 101196, https://doi.org/10.1016/j.jobe.2020.101196.

[19] L. Zalewski, S. Lassue, D. Rousse, K. Boukhalfa, Experimental and numerical characterization of thermal bridges in prefabricated building walls, Energy Convers. Manag. 51 (2010) 2869–2877, https://doi.org/10.1016/j.enconman.2010.06.026.

[20] F. Ascione, N. Bianco, R.F. De Masi, G.M. Mauro, M. Musto, G.P. Vanoli, Experimental validation of a numerical code by thin film heat flux sensors for the resolution of thermal bridges in dynamic conditions, Appl. Energy 124 (2014) 213–222, https://doi.org/10.1016/j.apenergy.2014.03.014.

[21] M.F. Alkadri, M.R.C. Agung, F. De Luca, An integrated computational method for calculating dynamic thermal bridges of building facades in tropical countries, Front. Architect. Res. 13 (2024) 201–218, https://doi.org/10.1016/j.foar.2023.11.003.

[22] H. Li, X. Zhang, H. Chen, D. Yang, H. Yang, Effect of thermal bridges on the thermal performance of embedded steel-framed autoclaved aerated concrete walls: experiments, analysis and design, J. Build. Eng. (2025) 113222, https://doi.org/10.1016/j.jobe.2025.113222.

[23] E. Iffa, D. Hun, M. Salonvaara, S. Shrestha, M. Lapsa, Performance evaluation of a dynamic wall integrated with active insulation and thermal energy storage systems, J. Energy Storage 46 (2022) 103815, https://doi.org/10.1016/j.est.2021.103815.

[24] European Organisation for Technical Approvals (EOTA), European Technical Approval ETA 10/0376, Kide Modular Cold Storage Room Kit, Catalonia Institute of Construction Technology (ITeC), Barcelona, Spain, 2013. Available at: https://www.itec.cat.

[25] EN 14509, Self-supporting Double Skin Metal Faced Insulating Panels – Factory Made Products – Specifications, European Committee for Standardization (CEN), Brussels, Belgium, 2013. Available at: https://itec.cat/.

[26] CEN, prEN 14509-1, Self-supporting double skin metal faced insulating panels – part 1: requirements for non-structural applications, in: Draft Standard, European Committee for Standardization, Brussels, 2024. Available at: https://standards.iteh.ai/catalog/standards/cen/6cccf966-f983-4108-96ce-f06a9d82e9c4/pren-14509-1.

[27] CEN, prEN 14509-2, Self-supporting double skin metal faced insulating panels – part 2: requirements for structural applications, in: Draft Standard, European Committee for Standardization, Brussels, 2024. Available at: https://standards.iteh.ai/catalog/standards/cen/ecfe63d1-d503-4b12-929b-d6bc1ad6d172/pren-14509-2.

[28] E. Vladimirova, M. Gong, Advancements and applications of wood-based sandwich panels in modern construction, Buildings 14 (2024) 2359, https://doi.org/10.3390/buildings14082359.

[29] A.M. Nanayakkara, S. Feih, A.P. Mouritz, Improving the fracture resistance of sandwich composite T-joints by z-pinning, Compos. Struct. 96 (2013) 207–215, https://doi.org/10.1016/j.compstruct.2012.09.029.

[30] H. Abdolpour, G. Escusa, J.M. Sena-Cruz, I.B. Valente, J.A. Barros, Axial performance of jointed sandwich wall panels, J. Compos. Constr. 21 (4) (2017) 04017009, https://doi.org/10.1061/(ASCE)CC.1943-5614.0000785.

[31] Ansys Release 2025 R1 Documentation for ANSYS Workbench. https://ansyshelp.ansys.com/public/Views/Secured/corp/v251/en/pdf/Workbench_Users_Guide.pdf, 2025.

[32] R. Kumar, D. Singh, A.K. Sharma, Static thermal analysis of fins models using Ansys, Int. J. Mech. Eng. Technol. 11 (2020) 10–21. http://www.iaeme.com/IJMET/issues.asp?JType=IJMET&VType=11&IType=2.

[33] R.W. Lewis, P. Nithiarasu, K.N. Seetharamu, Fundamentals of the Finite Element Method for Heat and Fluid Flow, John Wiley and Sons, 2004.

[34] M. Erturk, Z. Oktay, C. Coskun, G.A. Kilic, A. Dasdemir, A new approach to calculation of energy demand and amount of emission according to different indoor temperature, Int. J. Glob. Warm. 7 (2015) 395–408, https://doi.org/10.1504/IJGW.2015.069370.

[35] A. Hajjar, E. Jamesahar, H. Shirivand, M. Ghalambaz, R.B. Mahani, Transient phase change heat transfer in a metal foam-phase change material heatsink subject to a pulse heat flux, J. Energy Storage 31 (2020) 101701, https://doi.org/10.1016/j.est.2020.101701.

[36] Institut de Tecnologia de la Construcció de Catalunya (ITeC), European Technical Approval ETA 10/0376: KIDE Modular Cold Storage Room Kit, ITeC, 2010. Available online at, https://itec.es/certification/ete/issued.

[37] N. Hoivik, C. Greiner, J. Barragan, A.C. Iniesta, G. Skeie, P. Bergan, N. Calvet, Long-term performance results of concrete-based modular thermal energy storage system, J. Energy Storage 24 (2019) 100735, https://doi.org/10.1016/j.est.2019.04.009.